Influence of surfactant concentration on spontaneous emulsification kinetics

R Toor, R Denoyel, L Liggieri, M Schmitt, M Antoni

Influence of surfactant concentration on spontaneous emulsification kinetics

R. Toor[(1)], R. Denoyel[(1)], L. Liggieri[(2)], M. Schmitt[(1)] and M. Antoni[(1)]*

[(1)]Aix-Marseille Université, CNRS, MADIREL, Marseille, France

[(2)]CNR - Institute of Condensed Matter Chemistry and Technologies for Energy (ICMATE), Unit of Genoa, Italy

ABSTRACT : The kinetics of spontaneous emulsification is investigated on aqueous pendant drops in paraffin oil. Optical microscopy in transmission mode is used for high-spatial-resolution image recording. The influence of a lipophilic surfactant (Span 80) and two water-soluble surfactants (CTAB and SDS) is investigated. As time runs, the drops interface turns opaque due to the formation of microstructures associated with spontaneous emulsification. The time evolution of this phenomenon is shown to depend upon temperature and surfactant concentration which leads to an overall shrinkage due to gradual water uptake and transport into paraffin oil. Spontaneous emulsification kinetics depends upon the chemical composition. Higher concentration of Span 80 and CTAB (resp. SDS) are shown to promote (resp. hinder) water transport. This work provides new insights into the understanding of spontaneous emulsification when combining the properties of non-ionic and ionic surfactants.

Keywords: Spontaneous emulsification, water/oil interfaces, Span 80, CTAB, SDS, water transport.

1. Introduction

Emulsions have for long demonstrated their important potential for technological developments and industrial applications in various fields such as oil recovery , pharmaceutics [1,2], cosmetics [3,4], paint and food industry [5,6]. Common emulsions (or macroemulsions) consist of at least two immiscible liquids and are known to be thermodynamically unstable systems. They involve ageing mechanisms driven by buoyancy, drop/drop interactions, Ostw[7]ald ripening [8]. Kinetic stability over long time scales can however be achieved when adding surfactants and/or particles in the solutions. But for both thermodynamic and kinetic aspects, interfacial properties are paramount as they mostly govern all mass transfer mechanisms [9].

Emulsions can be generated by a variety of high or low energy methods [10–12]. High energy approaches involve the application of mechanical agitation with homogenizers, microfluidizers, ultrasonication [10,11] while low energy ones only depend on the physicochemical processes in play [13–15]. Low energy methods, such as spontaneous emulsification, are less invasive, making them very attractive to industry because of their obvious economic and societal benefits. They are of particular importance in the field of formulation where temperature control is often required in emulsification protocols.

Spontaneous emulsification (SE) results in the dispersion of one phase into another without external energy input [13]. It has been investigated extensively in a large variety of applications and emulsion types [15–21] since its discovery more than one century ago [22]. In spontaneous emulsifying systems, microstructures form, and their properties can be monitored by the chemicals that are used. They can for example behave as micro-reactors or provide efficient sol-gel synthesis routes for surfactant template-assisted mesostructured materials such as solid or hollow spheres [23], thins films [24] or high

surface area tubules [25]. Oil-in-water nano-emulsions can also be produced via SE [26] and offer important applications in drug delivery techniques [27–30].

Recent work focusing on pendant water drops in paraffin oil/Span 80 solutions revealed SE kinetics and evidenced the spontaneous occurrence of microstructures along the water/oil interface with typical morphology determined by the concentration in Span 80 [31]. Water transport from the drops into paraffin oil by reverse micelles was evidenced and shown to depend upon Span 80 concentration. When low (high), transport kinetics is slow (fast) and micrometer sized droplets (brush-like microstructures) are formed. As time runs, they multiply, swell and finally invade the whole interface. Water is therefore gradually removed from the drops leading to an overall decrease of their volume. Similar findings were already reported in literature [19,32]. SE studies with dodecane/Span 80 solutions have for example evidenced the generation of two dimensional colloidal structures made of spherical water droplets [33]. Spontaneous formation of water droplets was also observed with Span 80 for W/O/W (water/oil/water) emulsions [34].

The dynamic processes causing SE are still a matter for discussion. Two main ideas are proposed in the literature for their understanding: Mechanical breakup or chemical instability. Mechanical breakup can be caused by either interfacial turbulence or vanishing interfacial tension [35] while chemical instability can be promoted by bilayer collapse due to pressure gradients [36,37], local inversion of surfactant supersaturated regions [38,39] or chemical reactivity [40]. When mechanical breakup is the driving phenomenon, low surfactant concentrations are sufficient to evidence SE whereas, if chemical instability prevails, high surfactant concentrations are required and swelling of reverse micelles caused by chemical potential gradients is the driving mechanism.

The present study investigates SE in a system involving aqueous pendant drops suspended in paraffin oil with the aim of addressing the effect of composition changes. Non-ionic (Span 80, sorbitan monooleate), anionic (SDS, sodium dodecyl sulfate) and cationic (CTAB, cetyltrimethylammonium bromide) surfactants are considered. Synergetic effects of CTAB and SDS have been investigated for micro and nano-emulsion stability [41,42]. However, to our knowledge, never for systems experiencing SE. Span 80 will be used in all the experiments as SE has not been observed in its absence. Following this introductive section, section 2 will present the materials and methods employed. Section 3 concentrates on how SE kinetics is modified when changing Span 80 concentration. This section completes a previous investigation by taking fully into account a delay in SE attributed to the formation of surfactant monolayers [31]. Section 4 focuses on the combined effect of Span 80 and CTAB on one hand and Span 80 and SDS on the other. The possible underlying mechanisms responsible for SE changes in the presence of ionic surfactants is discussed. In the last section, conclusions and some perspectives are finally proposed.

2. Materials and methods

2.1. Materials

Span 80 was purchased from Fluka (catalog n. 09659). The HLB of 4.3 is reported for this surfactant, which is therefore soluble in non-polar solvents and often used to stabilize water-in-oil emulsions. Its CMC is 0.43 mM (0.18 - 0.26 g/L) at 20 °C in paraffin oil [43]. It consists ofa mixture of esters in the following fractions: sorbitan dioleate (36.5 %), Sorbitan triooleate (24.8 %), Sorbitan monooleate (19.1 %), Isosorbide monooleate (12.9 %) and Sorbitan tetraoleate (6.7 %). The presence of few unidentified components, which probably correspond to residues of the starting materials used for synthesis such as

oleic acid and sorbitol were also identified [44,45]. Hexadecyltrimethylammonium bromide (CTAB), pure to 99 %, was obtained from Sigma Aldrich (catalog n. 52365). CTAB is a cationic surfactant (HLB=10) with CMC of 1.0 mM (0.36 g/L) at 20 °C in water [46]. Sodium dodecyl sulfate (SDS) was purchased 99% pure from Sigma-Aldrich (catalog n. L3771). Its HLB is about 40 and its CMC is 8 mM (2.3 g/L) at 20 °C in water. Paraffin oil is provided by Sigma Aldrich (catalog n. 76235) and has density of 0.83 g/ml. All chemicals were used as supplied without any further purification. Water used for all the experiments was obtained from a Millipore Direct-Q water purification system (resistivity > 18,2 MΩ·cm, TOC < 5 ppb).

2.2. Sample preparation

The organic phase used here is paraffin oil (PO) loaded with Span 80. Fresh stock solutions are systematically used and prepared starting with a small amount of PO in a 100 mL volumetric flask. A given mass of Span 80, controlled by weighing of this flask, is added to reach the target stock solution concentration (10 g/L). The flask is filled up to the gauge line and the solution is homogenized by magnetic stirring at 600 rpm for 15 min at room temperature. Concentration of Span 80 is decreased by dilution down to 1 g/L. Concentrations are therefore always above CMC. The two ionic surfactants, CTAB and SDS, were used separately. Stock solutions for the aqueous phases are prepared by weighing and dissolution in water (total volume 50 mL) under magnetic stirring at 800 rpm for 30 min. The lower concentration solutions are then prepared by cascade dilutions of the stock solutions. For CTAB solutions, the studied concentration ranges between 0.01 g/L and 0.1 g/L (below CMC) while for SDS concentration is varied from 0.01 g/L to 1 g/L (also below CMC). The reason for using such moderate CTAB and SDS concentrations (when compared to the one of Span 80) results from the necessity to prevent interfacial tension to become too small. High SDS or CTAB concentrations make indeed pendant drop configurations unstable. They can deform, flow downward due to buoyancy and develop an unstable neck that eventually brings the drops to detach from the needle tip (see hereafter).

2.3. Experimental apparatus

Pendant drops (about 0.4 μL) of water are created at the end of a hydrophobic capillary needle. A Hamilton micro syringe (62 RN SYR, 2.5 μL) fitted with the needle is employed. Its tip is immersed in a 4 mL quartz cuvette previously filled with the chosen PO/Span 80 solution and covered with a stopper provided with a small hole to guide the needle and produce pendant drops centered in the field-of-view of a microscope. Typical images are shown in Figure 1. This sample cell is in a thermostat-controlled environmental chamber that can be moved with micrometric screws for the fine adjustment of centering. Temperature is controlled with a Peltier facility and a circulating bath granting temperature adjustments in the range -40°C to 100°C within ±0.5°C. The environmental chamber sits on an optical bench to limit the influence of uncontrolled external perturbations.

2.4. Optical microscopy and image analysis

The optical microscope is equipped with a 1024×1024-pixel CCD camera (Mikrotron, MC1310) encoded on 255 grey shades, allowing the observation of a magnified image corresponding to a field of

view (FOV) of 1×1 mm², with up to 500 Hz acquisition frame rate. The optical resolution of the microscope is therefore about 1 μm² per pixel. Light source is a LED producing a collimated light beam and a homogeneous background. The acquisition of images is started immediately after producing drops to capture early SE kinetics. Acquisition frame rate was set from 1 image every 5 seconds to about 1 image every 72 seconds depending on the experimental requirements. Sequences of several hundred images are produced by each experiment and post-processed using the Image-J Package with dedicated macros. Each image is binarized so as to be encoded on only two grey shades, white or black. A contrast-like function is then used to follow darkening/brightening of the images [31]:

$$f(t) = \frac{N(t)-N_{min}}{N(0)-N_{min}} \quad \text{(Eq. 1)}$$

where $N(t)$ (resp. $N(0)$) is the number of pixels with grey shades above 128 at time t (resp. initially). N_{min} is the minimum value reached by $N(t)$ in the processed image sequence. With this definition, $f(t)=1$ initially and $f(t)=0$ when the brightness of in the FOV is minimal. A decreasing (resp. increasing) trend of $f(t)$ is therefore the signature of an overall increasing (resp. decreasing) darkening of the images. f(t) is a quantity obtained by post processing of the images. It is measured over the complete FOV (1 mm²) and depends upon both the overall size of the pendant drop and the transparency of the water/paraffin oil interface. It is simple to define and has the great advantage of allowing straightforward quantitative measurements. For example, a shrinking of the size of the drop makes FOV brighter and therefore leads to an increase of its value. When considering light transmitted across the water/paraffin oil interface (ie. across the drop, see Figure 1), intensity depends upon the structure of the interface and upon the density of the scattering sites, here water microstructures, that the incident light beam meets along its optical path. The greater this density and the size of the microstructures, the more the transmitted intensity will be attenuated and therefore the smaller f(t) will be. Still, the definition of f(t), though practical, is limiting. It does not allow for example to discriminate the characteristic time associated with the densification kinetics of the microstructures on the interfaces from that associated with their swelling kinetics. It does not help either to probe the structure in depth of the water/paraffin oil interfaces. More precise techniques should be implemented, such as high-resolution tomographic microscopy, to achieve this level of description.

3. Results

3.1. Spontaneous emulsification at the water/paraffin oil interface

Figure 1 illustrates the evolution of a pendant drop for [Span 80] = 10 g/L at 30 °C. As the drop is under background illumination, its central area turns bright as expected from normal incidence. Initially, the interface between both liquids is smooth and the central area displays uniform illumination as shown in the magnified inset of Figure 1(a). As time runs, SE starts, and microstructures spontaneously develop with increasing crowding (Figure 1(b) and (c)). They are located at the interface, mostly consist of micrometer sized vesicles and act as scattering sites making the central area of the drop increasingly darker [31]. The formation of similar aggregate structures has recently been reported, but for a hydrophilic nonionic surfactant [47]. This evolution modifies the overall contrast of the images that is easy to track and quantify with $f(t)$ (Eq. (1)). Microstructures do not appear instantly and, depending upon Span 80 concentration, it may take minutes to hours for them to show up. It is therefore hypothesized that they are the result of the swelling of smaller objects produced at earlier time scales. Note that samples with Span 80 concentrations below CMC do not show such unusual

behavior when investigated over periods of several days [21]. In these last conditions, images keep similar to that of Figure 1(a) and show no significant change.

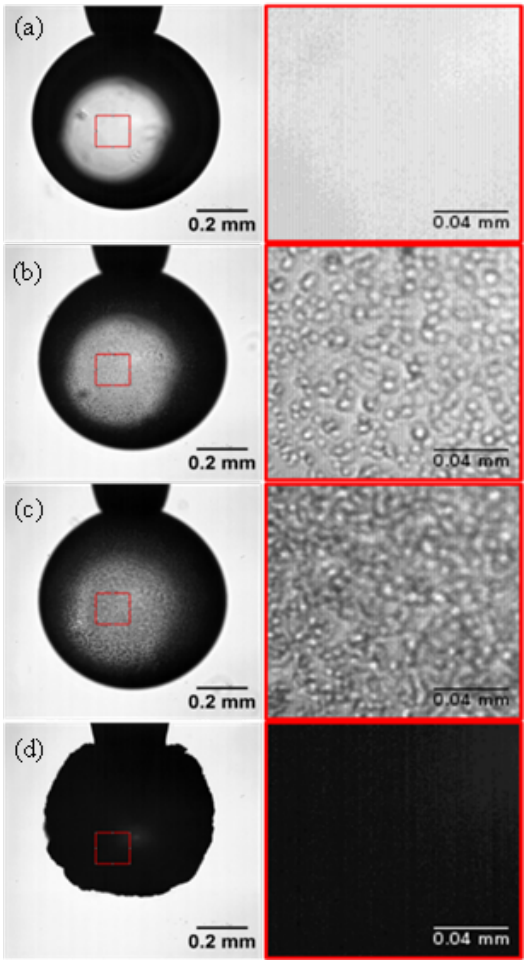

Figure 1. Left: Pictures (1 x 1 mm^2) of a pendant drop for [Span 80] = 10 g/L at 30 °C and at different times. (a) t = 0 s, (b) t = 1100 s and (c) t = 1400 s and (d) t = 10000 s. Right: Zoom in the selected region of interest (red square in right images).

Back to the results illustrated in Figure 1. Up to t=1400 s (Figure 1 (c)), the drop shows a progressive darkening, yet maintaining its initial size and axi-symmetry. Microstructures are produced, grow with time and gradually invade the whole interface as can be seen by a detailed inspection of the zooms of Figure 1(b) and (c). They flocculate and arrange in a compact network until densely packed. Cohesion forces remain strong enough for buoyancy or mechanical stress generated by swelling/flocculation to be small and microstructures to remain attached to the interface. Over longer periods of time, microstructures still develop but also start to detach. They behave as mobile objects dispersed in PO and transport water apart from the pendant drop similarly to what has been observed for capsules [40,48,49]. A new evolution regime sets then in where the initial drop axi-symmetry is lost as the drop undergoes shrinkage and deformation progressively. Deformation results here from non-isotropic interfacial stress generated by the progressive modification of the water/PO interface into a complex layer that looks very similar to a thin polymerized membrane [50]. As this phenomenon appears randomly on the interface, it produces drop shapes that can hardly be controlled. Eventually, drops appear as an opaque vesicle and water transport stops. Drops turn into vesicles consisting in a loose membrane of bounded microstructures through which water transport is no more possible (cf. Figure 1(d)).

Contrast function *f(t)* is employed to make the above discussion quantitative [31]. Figure 2(a) reports its evolution for three repetitions of the experiment illustrated in Figure 1. A decreasing trend is first observed. It vanishes when SE is sufficiently developed for the drops to prevent normal transmitted light. The curves of all three experiments overlap for t < 2500 s and therefore demonstrate good reproducibility. Drops keep axi-symmetric within this time interval. At longer time scales, *f(t)* increases as the shrinking and deformation of drops become measurable. Curves do not overlap anymore due to non-reproducible behavior resulting from the strong non-linearities in the microstructures interactions.

The average behavior of the three experiments, $\langle f(t) \rangle$, is plotted in Figure 2(b) for t < 2000 s. Three different SE regimes indicated as R_0, R_1 and R_2 are identified with characteristic times t_0, t_1 and t_2 defined by: $\langle f(t_0) \rangle = 0.95$, $\langle f(t_1) \rangle = 0.5$ and $\langle f(t_2) \rangle = 0.05$. R_0, R_1, and R_2 are typical of the behavior of the drops for the Span 80 concentration range investigated in this work (1 to 10 g/L) and provide important insights into SE typical time scales. R_0 corresponds to the initial lag stage of SE where no microstructures are observed under optical microscopy. This regime, that was not investigated in our previous work [31], takes place within time $t < t_0 \approx 1000$ s for [Span 80]=10 g/L and corresponds to the time needed for Span 80 molecules to diffuse from the PO solution onto the drops interface. R_0 is therefore an early-stage evolution period where molecular processes are creating the conditions for SE to be triggered. For the same Span 80 concentration, previous studies reported equilibration times of only few tens of second for the interfacial tension to achieve its value (about 5 mN/m). This is much shorter than the values of t_0 measured in this work and suggests that the mechanisms driving SE are already in action well before this time [37]. Optical microscopy is obviously not appropriate to catch molecular phenomena in action as R_0 takes place and this explains why $\langle f(t) \rangle$ remains almost unchanged. Complex time-dependent processes modifying the structure of the Span 80 adsorption layer, without having significant effects on its interfacial tension, cannot be excluded here [51,52]. Large surfactant concentrations as investigated here could moreover foster thick self-assemblies of complexes of water and oil which could, in turn, trigger SE [33,53]. In the second regime, R_1, drops turn dark due to increasing backlight scattering by ongoing SE creating a sharp decrease of $\langle f(t) \rangle$ when $t > t_0$. Microstructures increase in number and size while remaining attached onto the drop interface and densely packing. In the experimental conditions of Figure 2, $t_1 \approx 1300$ s and R_1 lasts up to time $t_2 \approx 1600$ s. Beyond this time, regime R_2 starts and drops turn completely opaque making the optical investigations no longer of interest. Direct visual observation however still indicates a rich phenomenology where microstructures continuously detach from the interface, creating free areas where new ones pop up. Simultaneously, the ones remaining attached to the interface continue to rearrange themselves in a way to generate layers with increasing compactness and roughness [31].

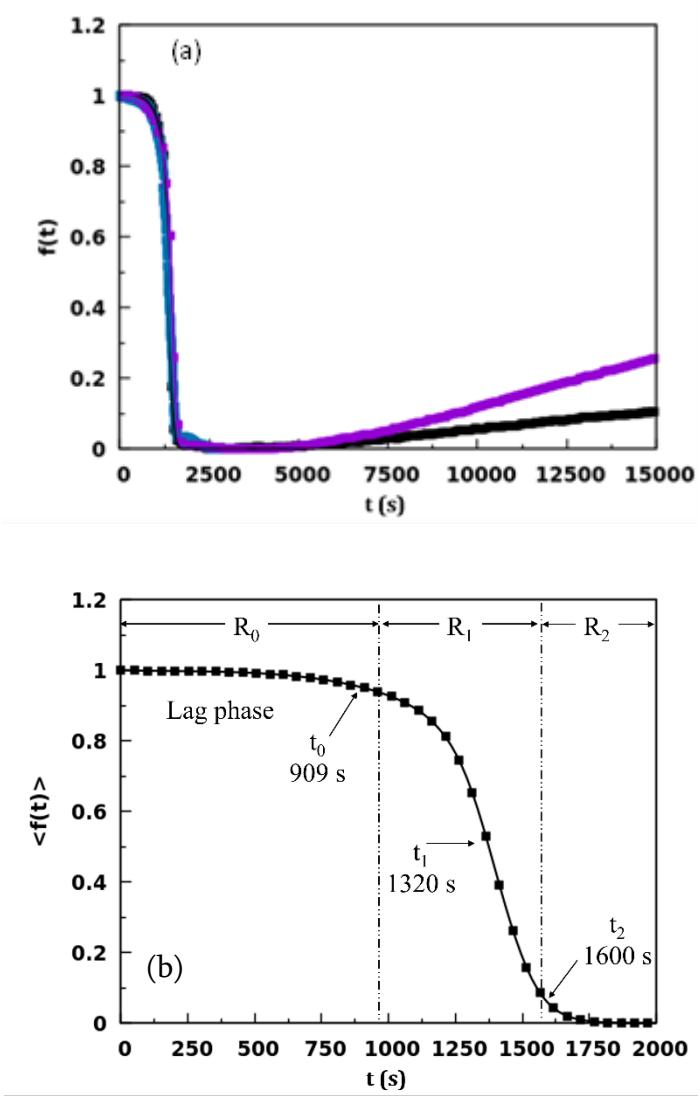

Figure 2. (a): Evolution of *f(t)* for [Span 80] = 10 g/L at 30°C up to t=15000 s for three identical experiments. Evolution becomes irreproducible once the drop undergoes shrinking (t > 2500 s). (b): Evolution of averaged fitted contrast function *<f(t)>* for the three experiments shown in (a) and time sequences associated to regimes R_0, R_1 and R_2.

To describe the role of Span 80 on SE kinetics, experiments were performed over a range of concentrations spanning from 1 g/L to 10 g/L. Figure 3 shows the behavior of t_0, t_1 and t_2 as a function of [Span 80]. Each measurement point is the average of at least three experiments. All three times decrease monotonously with increasing [Span 80] indicating that SE kinetics becomes faster. Changing [Span 80] from 1 g/L to 10 g/L leads for instance, to a decrease in t_1 from about 11000 s down to 1400 s. Full lines in Figure 3 result from a fitting of the data with a power law given in Eq. 2 (c_0=1g/L for homogeneity) and presented here to guide eyes. Fitting parameters t_{ref} and b are given in Table 1 and all indicate reasonable error ranges. As b ≈ -1, the characteristic times can be considered approximately as inversely proportional to the Span 80 concentration. Surprisingly, despite the complexity of the

interfacial molecular phenomena involved (see below), the global kinetics of the SE follows a rather simple law when changing composition.

$$t = t_{ref}\left(\frac{[\text{Span 80}]}{c_0}\right)^b \qquad \text{(Eq.2)}$$

	t_0	t_1	t_2
t_{ref} (s)	9635 ± 438	11007 ± 720	12781 ± 660
b	- 1.1 ± 0.1	- 0.9 ± 0.1	- 0.84 ± 0.1

Table 1 : Fitting parameters : t_{ref} and b (cf. Eq.2 and curves in Figure 3).

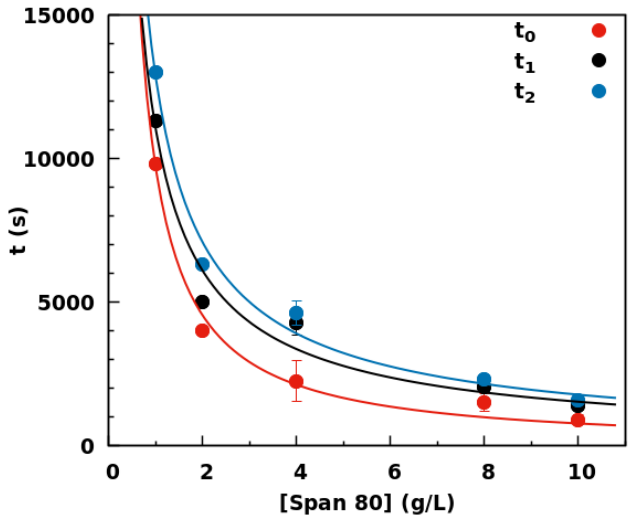

Figure 3. t_0, t_1 and t_2 as a function of [Span 80] at 30°C. Measurement points are the result of an average of at least three replica experiments. Errors bars are smaller than marker size when not visible.

The system investigated in this work is simple since it consists only of a pendant water drop, oil, and a lipophilic surfactant. But one still open question here is the understanding of the instability creating SE. As Span 80 concentration is much larger than CMC, it causes the formation of reverse micelles. Surfactant in the vicinity of the water/PO interface is therefore in large excess making bulk diffusion less effective in the overall kinetics of surfactant layer formation. Span 80 being a non-single component, all its constituents are expected, in principle, to contribute to SE processes and may involve surfactant/cosurfactant phenomena. To our knowledge, neither the ternary diagram of water/SPAN80/PO mixtures nor microscopic modelling of this system is available in the literature. Several mechanisms can be hypothesized to explain the very first step of SE. For instance, interfacial turbulence or a drastic decrease, or even a negative, interfacial tension resulting from Span 80 supersaturation. Diffusion and stranding may also come into play [44,45]. Another possible process relies on the formation of thick nonuniform multilamellar interfacial layers entrapping water films. Driven by chemical potential gradients, the latter could be fed by the drop water reservoir, swell until turning unstable most likely by Plateau-Rayleigh instability, and finally break off into microscopic objects [33,53]. All these mechanisms, if effective in SE, probably do coexist in a complex interplay as suggested by scanning electron microscopy analysis that revealed microstructures hierarchies consisting of protruding water vesicles at the water/oil interface [31]. Their shape depends on the Span 80

concentration and consists of either spheres or fibers depending on the Span 80 concentration. They grow in size and number, arranging themselves in a compact network while remaining attached to the interface. This is illustrated in the insets of Figure 1b and Figure 1c. It is also important to note here that no microstructure coalescence was evidenced. It is observed, instead, that small microstructures grow at the expense of the pendant drops, suggesting that Ostwald ripening clearly cannot be invoked to explain SE. The power spectra extracted from Figure 1b and Figure 1c (not shown here) indicate the presence of a peak corresponding to microstructures of characteristic size of 25+/-5 μm. This size is constant throughout the R_1 regime. Thus, the footprint of the microstructures on the drop interface remains nearly constant once they are in contact. The decrease in <f(t)> in R_1 (Figure 2(b)) can therefore be interpreted as a consequence of a growing complexity of the microstructures in the direction perpendicular to the drop interface[36].

Observations being done in transmission mode, optical distortions created by the curvature of the pendant drop and the proximity of the microstructures when densely packed should be accounted for here. <f(t)> is moreover an average quantity. It gives consequently an integrated information on the whole drop and optical path of the incident beam and therefore does not provide any relevant information on the structure of the interface at the microscopic scale. It would have been interesting here access to such a description while SE develops and in particular to observe the phenomena occurring on both sides of the interface[36]. Unfortunately, the transmission visualization technique used here does not allow such measurements. Preliminary tests on flat interfaces show that confocal microscopy may provide answers to this question. Span 80 has indeed detectable fluorescence. But addressing SE by this technique still requires important efforts. To have a sufficient magnification, the working distance must indeed be small (typically 2 mm) and this condition may produce experimental artifacts due to the proximity of solid surfaces. These measurements are still in progress and should allow, if successful, an in-situ study of the phenomena involved in SE.

The effect of temperature can be observed on comparing the time values at 30 °C in this work to those at 40 °C in our previous work [31]. For instance, Figure 3 shows that for [Span 80] = 10 g/L, $t_1 \approx 1300$ s at 30 °C and it decreases to $t_1 = 700$ s at 40 °C in the previous work [31]. SE becomes therefore faster at higher temperature. Viscosity of both paraffin oil and water decrease on increasing the temperature [54]. Temperature changes also modify relative solubility of surfactants, interfacial tensions, and bulk viscosity [55]. Faster SE is a straightforward consequence of enhanced Brownian motion of Span 80 that eases relaxation to local equilibrium and therefore naturally accelerates the overall SE kinetics. This trend is similar to the one described in foaming ability of surfactants when temperature is modified [56].

3.2. Influence of CTAB and SDS

The three regimes illustrated in Figure 2 still show up when CTAB or SDS is added to the aqueous phase and the three characteristic times t_0, t_1 and t_2 all show trends similar to the ones of Figure 3 when their concentration is changed (see Figure 4). This is the reason why forthcoming discussion will be limited to the description behavior of t_1 only. Maximal CTAB (resp. SDS) concentration is 0.08 g/L (resp. 0.3 g/L) here for stability purposes. For larger values interfacial tension becomes indeed too small, pendant drops get elongated due to buoyancy and detach from the capillary tip after few seconds. Note that both values do depend upon Span 80 in the concentration range investigated in this study. CTAB and SDS concentrations being smaller than their CMC, the pendant drop/PO interface is not compactly covered. As already discussed in the previous section for Span 80, SE kinetics depends on how fast

layers form, compete, and eventually get reorganized. The comparatively fast stability loss illustrated in Figure S3suggests that the formation of CTAB (or SDS) and Span 80 layers are most likely successive processes.

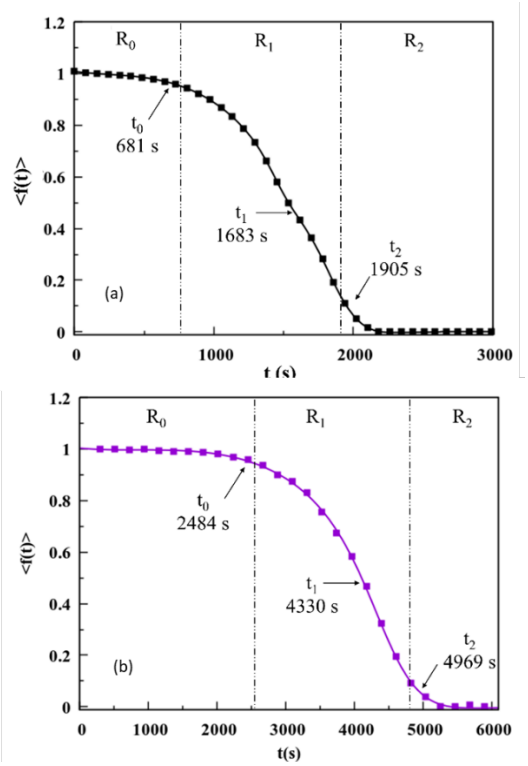

Figure 4. Evolution of <f(t)> for [Span 80] = 4 g/L at T=40°C. (a) [CTAB] = 0.06 g/L. (b) [SDS] = 0.3 g/L.

Figure 5 displays the evolution of <f(t)> for [Span 80] = 10 g/L and for varying [CTAB]. The decaying trend is similar to that of Figure 2 but yet appears earlier for increasing [CTAB]. This is essentially explained by electrostatic interactions weakening. In the absence of surfactant, water-oil interfaces are negatively charged because of hydroxide ions adsorption [57–60]. Being cationic, CTAB reduces zeta potential and, as local electrostatic interactions are weakened, adsorption energy barrier is lowered which promotes Span 80 adsorption. A similar behavior of CTAB is known to modify nano-emulsions stability [41]. The trend of Figure 5 turns consistent with this loss of stability and suggest that nanostructures formed at the very beginning of SE become less stable for increasing CTAB concentration. CTAB and Span 80 therefore act in a way to displace the CTAB/Span 80/hydroxyl groups adsorption/co-adsorption quasi-equilibrium in the sense to favor Span 80 only, making zeta-potential even smaller and the overall water transfer faster.

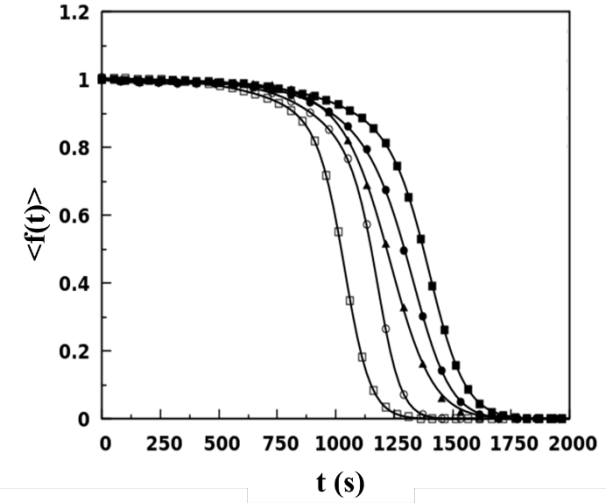

Figure 5. Evolution of <f(t)> as a function of [CTAB] for [Span 80] = 10 g/L at T=30°C. ■ [CTAB]=0 g/L, ● 0.02 g/L, ▲ 0.04 g/L, ○ 0.06 g/L and □ 0.08 g/L.

The above discussion invoked only surface charge effects. Other contributions, like hydrophobic interactions or steric hindrance, were assumed to be negligible [41]. One way to verify this hypothesis is to investigate interfacial charge modifications with SDS. SDS being anionic, zeta-potential becomes now more negative when increasing its concentration, and in contrast to CTAB, SDS is expected to yield a slowing down of SE. Figure 6 illustrates the evolution of t_1 when the water of the drops contains CTAB only (a) and SDS only (b). It shows a decreasing (resp. increasing) linear trend for CTAB (resp. SDS). Both figures also demonstrate stronger sensitivity to CTAB and SDS for small Span 80 concentrations. This is consistent with the fact that CTAB adsorption results in a better neutralization of the water/PO interface charge, in respect to SDS adsorption, that is also reflected by a different stability of the corresponding emulsions. The results are also consistent with previous studies that investigated and reported the synergistic interactions between nonionic and cationic surfactants [61–63]. For instance, the adsorption of CTAB was enhanced due to the synergies between CTAB and TX-100 (Triton X-100, non-ionic surfactant) [64]. A similar behavior was also reported for the surfactant mixture of DDAB (didodecyldimethylammonium bromide, cationic surfactant) and Igepal CO-890 (polyoxyethylene-40 nonylphenyl ether, non-ionic surfactant) in oil-in-water (O/W) emulsion [65]. In fact, while CTAB and SDS are good emulsifiers, it turns that below CMC, CTAB is a less efficient O/W emulsion stabilizer [66,67] than SDS that provides very stable emulsions already at concentrations well below the CMC [68].

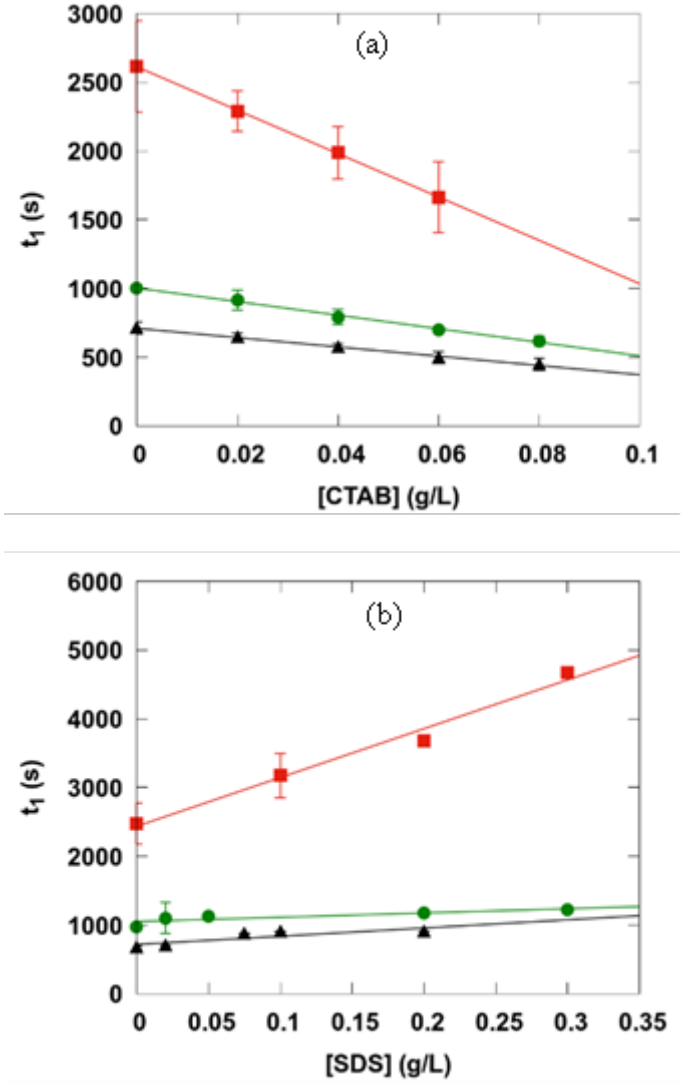

Figure 6. t_1 as a function of [CTAB] (a) and [SDS] (b) for three values of [Span 80] (■ 4 g/L, ● 8 g/L and ▲ 10 g/L) at T=40 °C. Error bars are smaller than markers when not visible.

4. Conclusions

This work provides new experimental insights into the complexity of spontaneous emulsification. Aqueous pendant drops suspended in a paraffin oil solution in the presence of non-ionic (Span 80) and ionic (CTAB and SDS) surfactants are studied. It is demonstrated that spontaneous emulsification generates microstructures at the water paraffin oil interface. For a given composition, three specific kinetic regimes mediated by the Span 80 concentration are identified. When adding CTAB (resp. SDS), SE kinetics turns faster (resp. slower). This change is explained by the polarity of water molecules and the modification in water/paraffin oil zeta potential associated with the ionic surfactants. CTAB tends in fact to reduce the zeta-potential and therefore facilitates the migration of water molecules while the SDS reinforces zeta-potential. Electrostatic interaction being strengthened, water transport is hindered, producing a delay in the occurrence of spontaneous emulsification. This work brings new insights and should help the understanding into possible mechanisms involved in spontaneous emulsification when ionic and non-ionic surfactants are in competition.

Acknowledgements

The authors acknowledge the financial support of CNES - Centre National des Etudes Spatiales - within the project 'Stabilité des Emulsions – Mesures et modélisation' and ESA - European Space Agency, within the project 'EDDI-Emulsion Dynamics and Droplet Interfaces – EDDI', ESA Contract n. 4000128643/19/NL/PG and M. Yvan CECERES from MADIREL for important technical support.

References

(1) Ahnfelt, E.; Degerstedt, O.; Lilienberg, E.; Sjögren, E.; Hansson, P.; Lennernäs, H. Lipiodol-Based Emulsions Used for Transarterial Chemoembolization and Drug Delivery: Effects of Composition on Stability and Product Quality. **2019**. https://doi.org/10.1016/j.jddst.2019.101143.

(2) Laredj-Bourezg, F.; Bolzinger, M. A.; Pelletier, J.; Chevalier, Y. Pickering Emulsions Stabilized by Biodegradable Block Copolymer Micelles for Controlled Topical Drug Delivery. *Int. J. Pharm.* **2017**, *531* (1), 134–142. https://doi.org/10.1016/j.ijpharm.2017.08.065.

(3) Gilbert, L.; Loisel, V.; Savary, G.; Grisel, M.; Picard, C. Stretching Properties of Xanthan, Carob, Modified Guar and Celluloses in Cosmetic Emulsions. *Carbohydr. Polym.* **2013**, *93* (2), 644–650. https://doi.org/10.1016/j.carbpol.2012.12.028.

(4) Bouchemal, K.; Briançon, S.; Perrier, E.; Fessi, H. Nano-Emulsion Formulation Using Spontaneous Emulsification: Solvent, Oil and Surfactant Optimisation. *Int. J. Pharm.* **2004**, *280* (1–2), 241–251. https://doi.org/10.1016/j.ijpharm.2004.05.016.

(5) Piorkowski, D. T.; Mcclements, D. J. Beverage Emulsions: Recent Developments in Formulation, Production, and Applications. **2013**. https://doi.org/10.1016/j.foodhyd.2013.07.009.

(6) Soo Lim, S.; Yeol Baik, M.; Andrew Decker, E.; Henson, L.; Michael Popplewell, L.; Julian McClements, D.; Jun Choi, S. Stabilization of Orange Oil-in-Water Emulsions: A New Role for Ester Gum as an Ostwald Ripening Inhibitor. **2011**. https://doi.org/10.1016/j.foodchem.2011.04.008.

(7) Afolabi, R. O.; Oluyemi, G. F.; Officer, S.; Ugwu, J. O. Hydrophobically Associating Polymers for Enhanced Oil Recovery – Part A: A Review on the Effects of Some Key Reservoir Conditions. *Journal of Petroleum Science and Engineering*. Elsevier B.V. September 2019, pp 681–698. https://doi.org/10.1016/j.petrol.2019.06.016.

(8) Binks, B. P. *Modern Aspects of Emulsion Science*; Binks, B. P., Ed.; Royal Society of Chemistry: Cambridge, 2007. https://doi.org/10.1039/9781847551474.

(9) Ravera, F.; Dziza, K.; Santini, E.; Cristofolini, L.; Liggieri, L. Emulsification and Emulsion Stability: The Role of the Interfacial Properties. *Adv. Colloid Interface Sci.* **2021**, *288*, 102344. https://doi.org/https://doi.org/10.1016/j.cis.2020.102344.

(10) Lignel, S.; Salsac, A. V.; Drelich, A.; Leclerc, E.; Pezron, I. Water-in-Oil Droplet Formation in a Flow-Focusing Microsystem Using Pressure- and Flow Rate-Driven Pumps. *Colloids Surfaces A Physicochem. Eng. Asp.* **2017**, *531* (May), 164–172. https://doi.org/10.1016/j.colsurfa.2017.07.065.

(11) McClements, D. J.; Rao, J. Food-Grade Nanoemulsions: Formulation, Fabrication, Properties, Performance, Biological Fate, and Potential Toxicity. *Crit. Rev. Food Sci. Nutr.* **2011**, *51* (4), 285–330. https://doi.org/10.1080/10408398.2011.559558.

(12) Leong, T. S. H.; Wooster, T. J.; Kentish, S. E.; Ashokkumar, M. Minimising Oil Droplet Size Using Ultrasonic Emulsification. *Ultrason. Sonochem.* **2009**, *16* (6), 721–727. https://doi.org/10.1016/j.ultsonch.2009.02.008.

(13) Solans, C.; Solé, I. Nano-Emulsions: Formation by Low-Energy Methods. *Curr. Opin. Colloid Interface Sci.* **2012**, *17* (5), 246–254. https://doi.org/10.1016/j.cocis.2012.07.003.

(14) Solans, C.; Morales, D.; Homs, M. Spontaneous Emulsification. *Current Opinion in Colloid and Interface Science*. 2016, pp 88–93. https://doi.org/10.1016/j.cocis.2016.03.002.

(15) Zhao, S.; Tian, G.; Zhao, C.; Li, C.; Bao, Y.; DiMarco-Crook, C.; Tang, Z.; Li, C.; Julian McClements, D.; Xiao, H.; Zheng, J. The Stability of Three Different Citrus Oil-in-Water Emulsions Fabricated by Spontaneous Emulsification. *Food Chem.* **2018**, *269* (December 2017), 577–587. https://doi.org/10.1016/j.foodchem.2018.07.062.

(16) Miller, C. A. Spontaneous Emulsification Produced by Diffusion - A Review. *Colloids and Surfaces* **1988**, *29* (1), 89–102. https://doi.org/10.1016/0166-6622(88)80173-2.

(17) Li, Z.; Xu, D.; Yuan, Y.; Wu, H.; Hou, J.; Kang, W.; Bai, B. Advances of Spontaneous Emulsification and Its Important Applications in Enhanced Oil Recovery Process. *Adv. Colloid Interface Sci.* **2020**, *277*, 102119. https://doi.org/https://doi.org/10.1016/j.cis.2020.102119.

(18) Riehm, D. A.; Rokke, D. J.; Paul, P. G.; Lee, H. S.; Vizanko, B. S.; McCormick, A. V. Dispersion of Oil into Water Using Lecithin-Tween 80 Blends: The Role of Spontaneous Emulsification. *J. Colloid Interface Sci.* **2017**, *487*, 52–59. https://doi.org/10.1016/j.jcis.2016.10.010.

(19) Bahtz, J.; Gunes, D. Z.; Hughes, E.; Pokorny, L.; Riesch, F.; Syrbe, A.; Fischer, P.; Windhab, E. J. Decoupling of Mass Transport Mechanisms in the Stagewise Swelling of Multiple Emulsions. **2015**. https://doi.org/10.1021/acs.langmuir.5b01138.

(20) Wen, L.; Papadopoulos, K. D. Effects of Osmotic Pressure on Water Transport in W1/O/W2 Emulsions. *J. Colloid Interface Sci.* **2001**, *235* (2), 398–404. https://doi.org/https://doi.org/10.1006/jcis.2000.7384.

(21) Silva, P. S.; Zhdanov, S.; Starov, V. M.; Holdich, R. G. Spontaneous Emulsification of Water in Oil at Appreciable Interfacial Tensions. *Colloids Surfaces A Physicochem. Eng. Asp.* **2017**, *521*, 141–146. https://doi.org/https://doi.org/10.1016/j.colsurfa.2016.05.041.

(22) Gad, J. Zur Lehre von Der Blutrache. *Arch. Anat. Physiol., Lpz.* **1878**, 181–192.

(23) Andersson, N.; Kronberg, B.; Corkery, R.; Alberius, P. Combined Emulsion and Solvent Evaporation (ESE) Synthesis Route to Well-Ordered Mesoporous Materials. *Langmuir* **2007**, *23* (3), 1459–1464.

(24) Walcarius, A.; Sibottier, E.; Etienne, M.; Ghanbaja, J. Electrochemically Assisted Self-Assembly of Mesoporous Silica Thin Films. *Nat. Mater.* **2007**, *6* (8), 602–608. https://doi.org/10.1038/nmat1951.

(25) Peng, T.; Hasegawa, A.; Qiu, J.; Hirao, K. Fabrication of Titania Tubules with High Surface Area and Well-Developed Mesostructural Walls by Surfactant-Mediated Templating Method. *Chem. Mater.* **2003**, *15*. https://doi.org/10.1021/cm020828f.

(26) Solè, I.; Solans, C.; Maestro, A.; González, C.; Gutiérrez, J. M. Study of Nano-Emulsion Formation by Dilution of Microemulsions. *J. Colloid Interface Sci.* **2012**, *376* (1), 133–139. https://doi.org/10.1016/j.jcis.2012.02.063.

(27) Saberi, A. H.; Fang, Y.; McClements, D. J. Fabrication of Vitamin E-Enriched Nanoemulsions: Factors Affecting Particle Size Using Spontaneous Emulsification. *J. Colloid Interface Sci.* **2013**, *391* (1), 95–102. https://doi.org/10.1016/j.jcis.2012.08.069.

(28) Saberi, A. H.; Fang, Y.; McClements, D. J. Effect of Salts on Formation and Stability of Vitamin E-Enriched Mini-Emulsions Produced by Spontaneous Emulsification. *J. Agric. Food Chem.* **2014**, *62* (46), 11246–11253. https://doi.org/10.1021/jf503862u.

(29) Guttoff, M.; Saberi, A. H.; Mcclements, D. J. Formation of Vitamin D Nanoemulsion-Based

Delivery Systems by Spontaneous Emulsification : Factors Affecting Particle Size and Stability. **2015**, *171*, 117–122.

(30) Date, A. A.; Desai, N.; Dixit, R.; Nagarsenker, M. Self-Nanoemulsifying Drug Delivery Systems: Formulation Insights, Applications and Advances. *Nanomedicine* **2010**, *5* (10), 1595–1616. https://doi.org/10.2217/nnm.10.126.

(31) Schmitt, M.; Toor, R.; Denoyel, R.; Antoni, M. Spontaneous Microstructure Formation at Water/Paraffin Oil Interfaces. *Langmuir* **2017**, *33* (49), 14011–14019. https://doi.org/10.1021/ACS.LANGMUIR.7B02549.

(32) Bahtz, J.; Gunes, D. Z.; Syrbe, A.; Mosca, N.; Fischer, P.; Windhab, E. J. Quantification of Spontaneous W/O Emulsification and Its Impact on the Swelling Kinetics of Multiple W/O/W Emulsions. *Langmuir* **2016**, *32* (23), 5787–5795. https://doi.org/10.1021/acs.langmuir.6b00425.

(33) González-Ochoa, H.; Arauz-Lara, J. L. Spontaneous Two-Dimensional Spherical Colloidal Structures. *Langmuir* **2007**, *23* (10), 5289–5291. https://doi.org/10.1021/la070144s.

(34) Wen, L.; Papadopoulos, K. D. Effects of Surfactants on Water Transport in W1/O/W2 Emulsions. *Langmuir* **2000**, *16* (20), 7612–7617. https://doi.org/10.1021/la000071b.

(35) Dabros, T.; Yeung, A.; Masliyah, J.; Czarnecki, J. Emulsification through Area Contraction. *J. Colloid Interface Sci.* **1999**, *210* (1), 222–224. https://doi.org/https://doi.org/10.1006/jcis.1998.5943.

(36) Shahidzadeh, N.; Bonn, D.; Meunier, J.; Nabavi, M.; Airiau, M.; Morvan, M. Dynamics of Spontaneous Emulsification for Fabrication of Oil in Water Emulsions. *Langmuir* **2000**, *16* (25), 9703–9708. https://doi.org/10.1021/la000493l.

(37) Shahidzadeh, N.; Bonn, D.; Meunier, J. A New Mechanism of Spontaneous Emulsification: Relation to Surfactant Properties. *Europhys. Lett.* **1997**, *40* (4), 459–464. https://doi.org/10.1209/epl/i1997-00488-0.

(38) Greiner, R. W.; Evans, D. F. Spontaneous Formation of a Water-Continuous Emulsion from a w/o Microemulsion. *Langmuir* **1990**, *6* (12), 1793–1796. https://doi.org/10.1021/la00102a014.

(39) Ruschak, K. J.; Miller, C. A. Spontaneous Emulsification in Ternary Systems with Mass Transfer. *Ind. Eng. Chem. Fundam.* **1972**, *11* (4), 534–540. https://doi.org/10.1021/i160044a017.

(40) Nishimi, T.; Miller, C. A. Spontaneous Emulsification Produced by Chemical Reactions. *J. Colloid Interface Sci.* **2001**, *237* (2), 259–266. https://doi.org/https://doi.org/10.1006/jcis.2001.7467.

(41) Xin, X.; Zhang, H.; Xu, G.; Tan, Y.; Zhang, J.; Lv, X. Influence of CTAB and SDS on the Properties of Oil-in-Water Nano-Emulsion with Paraffin and Span 20/Tween 20. *Colloids Surfaces A Physicochem. Eng. Asp.* **2013**, *418*, 60–67. https://doi.org/https://doi.org/10.1016/j.colsurfa.2012.10.065.

(42) Zdrali, E.; Etienne, G.; Smolentsev, N.; Amstad, E.; Roke, S. The Interfacial Structure of Nano- and Micron-Sized Oil and Water Droplets Stabilized with SDS and Span80. *J. Chem. Phys.* **2019**, *150* (20), 204704. https://doi.org/10.1063/1.5083844.

(43) Santini, E.; Liggieri, L.; Sacca, L.; Clausse, D.; Ravera, F. Interfacial Rheology of Span 80 Adsorbed Layers at Paraffin Oil-Water Interface and Correlation with the Corresponding Emulsion Properties. *Colloids Surfaces A Physicochem. Eng. Asp.* **2007**, *309* (1–3), 270–279. https://doi.org/10.1016/j.colsurfa.2006.11.041.

(44) Abou-Nemeh, I.; Van Peteghem, A. P. Some Aspects of Emulsion Instability on Using Sorbitan Monooleate (Span 80) as a Surfactant in Liquid Emulsion Membranes. *Chemie Ing. Tech.* **1990**, *62* (5), 420–421. https://doi.org/10.1002/cite.330620520.

(45) Abou-Nemeh, I.; Van Peteghem, A. P. Sorbitan Monooleate (Span 80) Decomposition during Membrane Ageing. A Kinetic Study. *J. Memb. Sci.* **1992**, *74* (1–2), 9–17. https://doi.org/10.1016/0376-7388(92)87068-9.

(46) van Os, N. M.; Haak, J. R.; Rupert, L. A. M. *Physico-Chemical Properties of Selected Anionic, Cationic and Nonionic Surfactants*; Elsevier, 2012.

(47) Hu, X.; Binks, B. P.; Cui, Z. High Internal Phase Emulsions Stabilized by Adsorbed Sucrose Stearate Molecules and Dispersed Vesicles. *Food Hydrocoll.* **2021**, *121*, 107002. https://doi.org/https://doi.org/10.1016/j.foodhyd.2021.107002.

(48) Fessi, H.; Puisieux, F.; Devissaguet, J. P.; Ammoury, N.; Benita, S. Nanocapsule Formation by Interfacial Polymer Deposition Following Solvent Displacement. *Int. J. Pharm.* **1989**, *55* (1), R1–R4. https://doi.org/https://doi.org/10.1016/0378-5173(89)90281-0.

(49) Quintanar-Guerrero, D.; Allémann, E.; Doelker, E.; Fessi, H. A Mechanistic Study of the Formation of Polymer Nanoparticles by the Emulsification-Diffusion Technique. *Colloid Polym. Sci.* **1997**, *275* (7), 640–647. https://doi.org/10.1007/s003960050130.

(50) Wiese, K. J. *Polymerized Membranes, a Review*; Domb, C.; Lebowitz, J. L., Eds.; Phase Transitions and Critical Phenomena, Vol. 19; Academic Press, London, 2000.

(51) Ravera, F.; Ferrari, M.; Liggieri, L. Modelling of Dilational Visco-Elasticity of Adsorbed Layers with Multiple Kinetic Processes. *Colloids Surfaces A Physicochem. Eng. Asp.* **2006**, *282–283* (Complete), 210–216. https://doi.org/10.1016/j.colsurfa.2005.11.066.

(52) Ravera, F.; Ferrari, M.; Santini, E.; Liggieri, L. Influence of Surface Processes on the Dilational Visco-Elasticity of Surfactant Solutions. *Adv. Colloid Interface Sci.* **2005**, *117* (1–3), 75–100. https://doi.org/10.1016/j.cis.2005.06.002.

(53) Pautot, S.; Frisken, B. J.; Cheng, J.-X.; Xie, X. S.; Weitz, D. A. Spontaneous Formation of Lipid Structures at Oil/Water/Lipid Interfaces. *Langmuir* **2003**, *19* (24), 10281–10287. https://doi.org/10.1021/la034532f.

(54) Fujiu, K. B.; Kobayashi, I.; Neves, M. A.; Uemura, K.; Nakajima, M. Influence of Temperature on Production of Water-in-Oil Emulsions by Microchannel Emulsification. *Colloids Surfaces A Physicochem. Eng. Asp.* **2012**, *411*, 50–59. https://doi.org/10.1016/j.colsurfa.2012.07.001.

(55) Kovalchuk, V. I.; Loglio, G.; Bykov, A. G.; Ferrari, M.; Krägel, J.; Liggieri, L.; Miller, R.; Milyaeva, O. Y.; Noskov, B. A.; Ravera, F.; Santini, E.; Schneck, E. Effect of Temperature on the Dynamic Properties of Mixed Surfactant Adsorbed Layers at the Water/Hexane Interface under Low-Gravity Conditions. *Colloids and Interfaces* **2020**, *4* (3). https://doi.org/10.3390/colloids4030027.

(56) Wang, H.; Guo, W.; Zheng, C.; Wang, D.; Zhan, H. Effect of Temperature on Foaming Ability and Foam Stability of Typical Surfactants Used for Foaming Agent. *J. Surfactants Deterg.* **2017**, *20* (3), 615–622. https://doi.org/10.1007/S11743-017-1953-9.

(57) Marinova, K. G.; Alargova, R. G.; Denkov, N. D.; Velev, O. D.; Petsev, D. N.; Ivanov, I. B.; Borwankar, R. P. Charging of Oil-Water Interfaces Due to Spontaneous Adsorption of Hydroxyl Ions. *Langmuir* **1996**, *12* (8), 2045–2051.

(58) Vácha, R.; Rick, S. W.; Jungwirth, P.; De Beer, A. G. F.; De Aguiar, H. B.; Samson, J. S.; Roke, S. The Orientation and Charge of Water at the Hydrophobic Oil Droplet–Water Interface. *J. Am. Chem. Soc.* **2011**, *133* (26), 10204–10210. https://doi.org/10.1021/JA202081X.

(59) Beattie, J. K.; Djerdjev, A. M. The Pristine Oil/Water Interface: Surfactant-Free Hydroxide-Charged Emulsions. *Angew. Chemie Int. Ed.* **2004**, *43* (27), 3568–3571. https://doi.org/10.1002/ANIE.200453916.

(60) Ma, A.; Xu, J.; Xu, H. Impact of Spontaneously Adsorbed Hydroxide Ions on Emulsification via

Solvent Shifting. *J. Phys. Chem. C* **2014**, *118* (40), 23175–23180. https://doi.org/10.1021/jp5076109.

(61) Roque, L.; Fernández, M.; Benito, J. M.; Escudero, I. Stability and Characterization Studies of Span 80 Niosomes Modified with CTAB in the Presence of NaCl. *Colloids Surfaces A Physicochem. Eng. Asp.* **2020**, *601*, 124999. https://doi.org/https://doi.org/10.1016/j.colsurfa.2020.124999.

(62) Wiertel-Pochopien, A.; Batys, P.; Zawala, J.; Kowalczuk, P. B. Synergistic Effect of Binary Surfactant Mixtures in Two-Phase and Three-Phase Systems. *J. Phys. Chem. B* **2021**, *125* (15), 3855–3866. https://doi.org/10.1021/ACS.JPCB.1C00664/SUPPL_FILE/JP1C00664_SI_001.PDF.

(63) Zhang, Y.; Zhao, Y.; Zhu, Y.; Wu, H.; Wang, H.; Lu, W. Adsorption of Mixed Cationic-Nonionic Surfactant and Its Effect on Bentonite Structure. *J. Environ. Sci.* **2012**, *24* (8), 1525–1532. https://doi.org/10.1016/S1001-0742(11)60950-9.

(64) Hou, B.; Jia, R.; Fu, M.; Wang, Y.; Bai, Y.; Huang, Y. Wettability Alteration of an Oil-Wet Sandstone Surface by Synergistic Adsorption/Desorption of Cationic/Nonionic Surfactant Mixtures. *Energy and Fuels* **2018**, *32* (12), 12462–12468. https://doi.org/10.1021/ACS.ENERGYFUELS.8B03450/ASSET/IMAGES/ACS.ENERGYFUELS.8B03450.SOCIAL.JPEG_V03.

(65) Banerjee, B.; Paria, S. Effect of Electrolytes on Solution and Interfacial Behaviors of Double Chain Cationic-Nonionic Surfactant Mixtures for Hydrophobic Surface Wetting and Oil/Water Emulsion Stability Applications. *Langmuir* **2021**, *37* (35), 10560–10572. https://doi.org/10.1021/ACS.LANGMUIR.1C01672/SUPPL_FILE/LA1C01672_SI_001.PDF.

(66) Zhu, Y.; Jiang, J.; Liu, K.; Cui, Z.; Binks, B. P. Switchable Pickering Emulsions Stabilized by Silica Nanoparticles Hydrophobized in Situ with a Conventional Cationic Surfactant. *Langmuir* **2015**, *31* (11), 3301–3307. https://doi.org/10.1021/ACS.LANGMUIR.5B00295/SUPPL_FILE/LA5B00295_SI_001.PDF.

(67) Zhu, Y.; Chen, T.; Cui, Z.; Dai, H.; Cai, L. Stimuli-Responsive Biomass Cellulose Particles Being Able to Reversibly Self-Assemble at Fluid Interface. *Front. Chem.* **2020**, *8*, 712. https://doi.org/10.3389/fchem.2020.00712.

(68) Llamas, S.; Santini, E.; Liggieri, L.; Salerni, F.; Orsi, D.; Cristofolini, L.; Ravera, F. Adsorption of Sodium Dodecyl Sulfate at Water–Dodecane Interface in Relation to the Oil in Water Emulsion Properties. *Langmuir* **2018**, *34* (21), 5978–5989. https://doi.org/10.1021/acs.langmuir.8b00358.

For Table of Contents Use Only